Supporting Information

Splash-Resistant and Light-Weight Silk-Sheathed Wires for Textile Electronics

*Zhe Yin[a,b], Muqiang Jian[a,b], Chunya Wang[a,b], Kailun Xia[a,b], Zhehong Liu[c], Qi Wang[a,b], Mingchao Zhang[a,b], Huimin Wang[a,b], Xiaoping Liang[a,b], Xiao Liang[a], Youwen Long[c], Xiaohui Yu[c] and Yingying Zhang[a, b *]*

[a] Key Laboratory of Organic Optoelectronics and Molecular Engineering of the Ministry of Education, Department of Chemistry, Tsinghua University, Beijing 100084, People's Republic of China

[b] Center for Nano and Micro Mechanics, School of Aerospace Engineering, Tsinghua University, Beijing 100084, PR China

[c] Beijing National Laboratory for Condensed Matter Physics, Institute of Physics, Chinese Academy of Sciences, Beijing 100190, PR China

*Address correspondence to yingyingzhang@tsinghua.edu.cn

This supporting file includes:

- Supporting Notes S1 to S4
- Supporting Figures S1 to S11
- Supporting Table S1

The sequence is the same as they are mentioned in the main text.

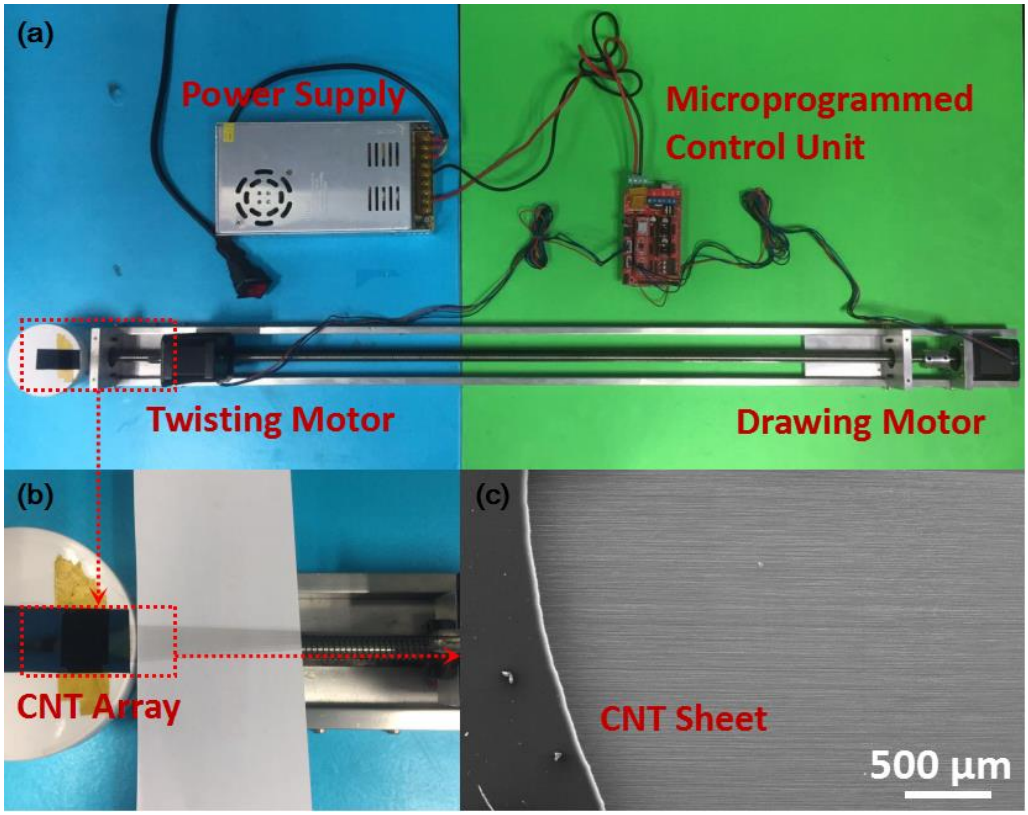

Figure S1. Experimental setup for the preparation of CNT yarn. (a) Overview of the machine setup. The microprogrammed control unit is Arduino Mega 2560. (b) The rotating motor for twisting. (c) SEM image of the CNT sheet.

Note S1. Electrospinning and rotating

Electrospinning of silk nanofibers

The silk nanofibers ejected from the needle, forming a Taylor Cone above the rotating CNT yarn. Then the ejected electrospun silk nanofibers wrapped around the rotating CNT yarn.

Rotating of a CNT yarn

The rotating and collecting operations were realized by three motors (two rotating motors and one collecting motor), which rotated at differential speeds, causing the yarn to be wound onto the collector. The two rotating motors rolled in the same direction at the same speed, as marked by the green arrows. The setup was based on a reported prototype. More details can be found in the reference.[1]

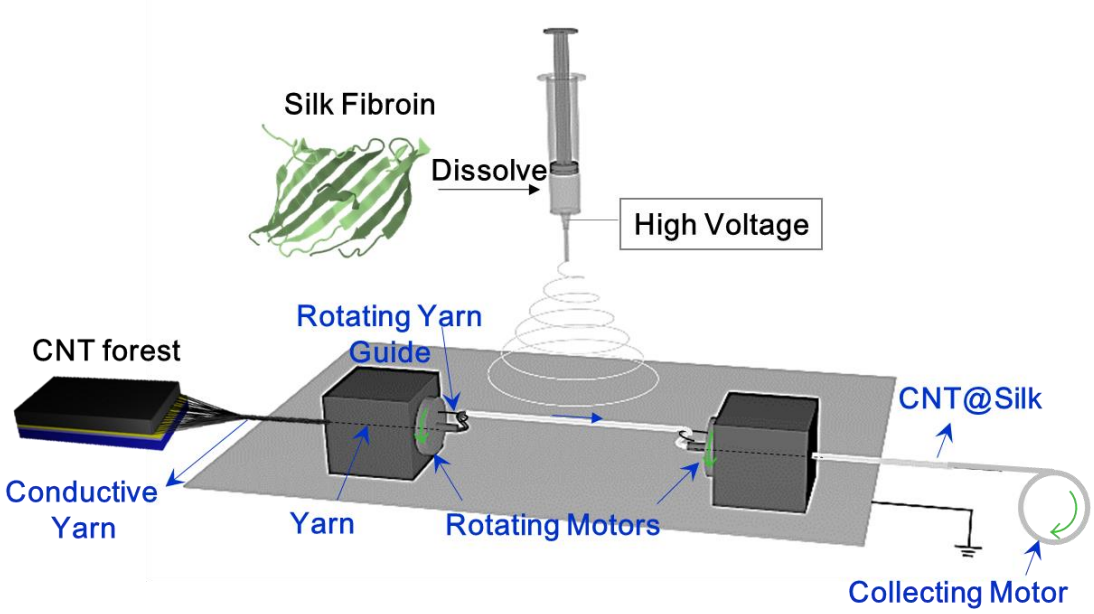

Figure S2. Schematic illustration showing the fabrication of the CNT@Silk wire by deposition of electrospun silk nanofibers on a rotating CNT yarn.

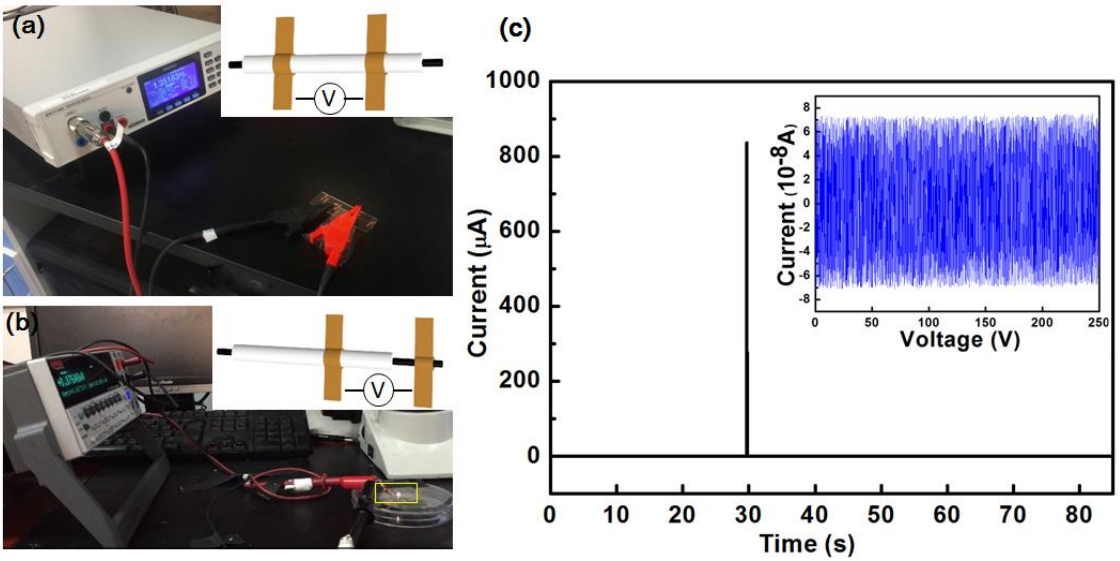

Figure S3. Electrical insulation test of the silk sheath. (a) High resistance calibrator for measuring the resistance of the sheath. The inset illustrates the sample with the silk sheath connected to electrodes. (b) Measuring the breakdown voltage of the silk sheath using a Keithley 2410. The yellow box indicates the spark at voltage breakdown. The inset illustrates the sample with the silk sheath and CNT core connected to electrodes, respectively. (c) The

current-time curve for the breakdown voltage measurement in (b). The inset is the magnified current-voltage curve.

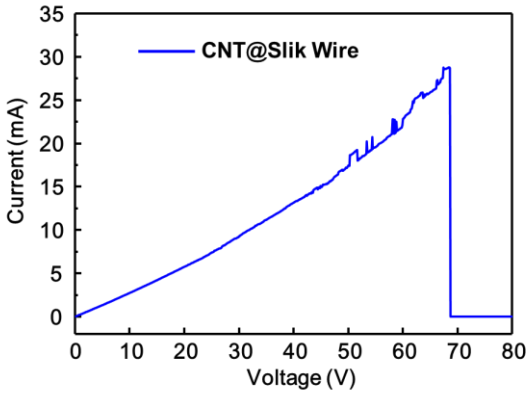

Figure S4. Electrical tests. Current-voltage curve of a CNT@Silk wire (length: 18 mm; diameter: 13± 1 μm), showing that it can sustain a current as high as 28 mA at a voltage of 68.6 V.

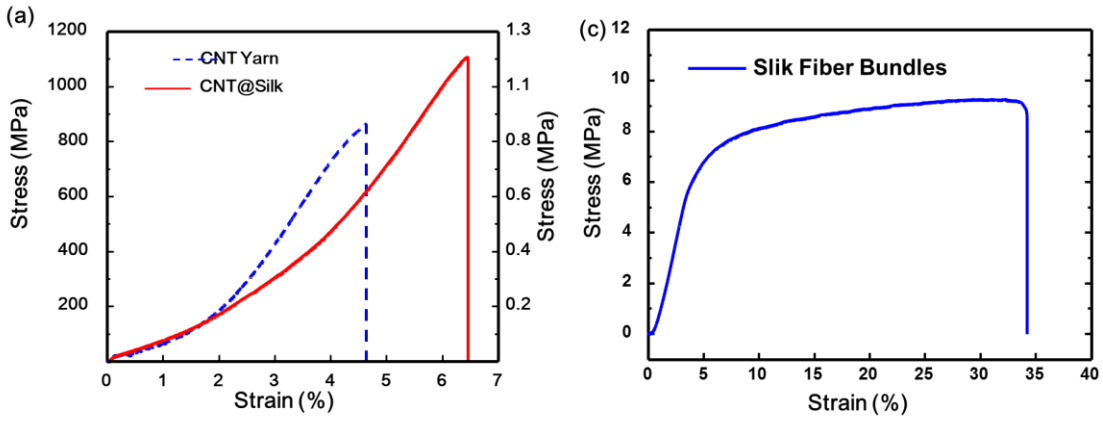

Figure S5. Mechanical tests. (a) Strength−strain curves of a bare CNT yarn and a CNT@Silk wire. The left y-axis corresponds to the stress of a CNT yarn and a CNT@Silk wire calculated according to the cross section of the CNT core. The right y-axis corresponds to the stress of a wire calculated according to the entire cross section of the CNT@Silk wire. (b) Stress-strain curve of a yarn composed of pure electrospun silk fibers.

Table S1. Comparison of the mechanical properties of CNT yarns in this work and reported CNT yarns/fibers.

CNT Yarns/Fibers	*Synthesis*	*Tensile Strength*	*Elongation at Break*	*Reference*
1	Dry-spun	843±80 MPa	4.7±0.4%	This work
2	Dry-spun	850 MPa	2.2%	2
3	Dry-spun	300 MPa	7.5%	3
4	Dry-spun	1.3-3.3 GPa	2-9%	4
5	Wet-spun	1±0.2 GPa	1.4±0.5%	5
6	Wet-spun	150 MPa	3%	6
7	Floating CVD	800 MPa	<8%	7

Note S2. Wear resistance test

According to a reported wear resistance test approach,[8] we designed a home-made setup to do the wear resistance test. We used a Cu wire as a translating fiber and the CNT@Silk wire as a stationary fiber. The Cu wire contacted with the CNT@Silk wire at the crossover and the Cu wire moved up and down to abrase the tested CNT@Silk wire. To accelerate the testing, we used an abrasive paper to roughen the surface of Cu wire first (Figure S6b). As shown in Movie R1, the Cu wire moves at a speed of 4 mm/s and the distance of each moving cycle is 8 mm. During the testing, a voltage of 0.1 V was applied between the Cu wire and the CNT@Silk wire. The current and the friction force between the two wires was monitored. When the silk sheath wears out, the Cu wire and the CNT fiber are connected and a current between the Cu wire and the CNT core will be observed (Figure S7). The results show that the silk sheath can withstand the abrasion for more than 5400 cycles.

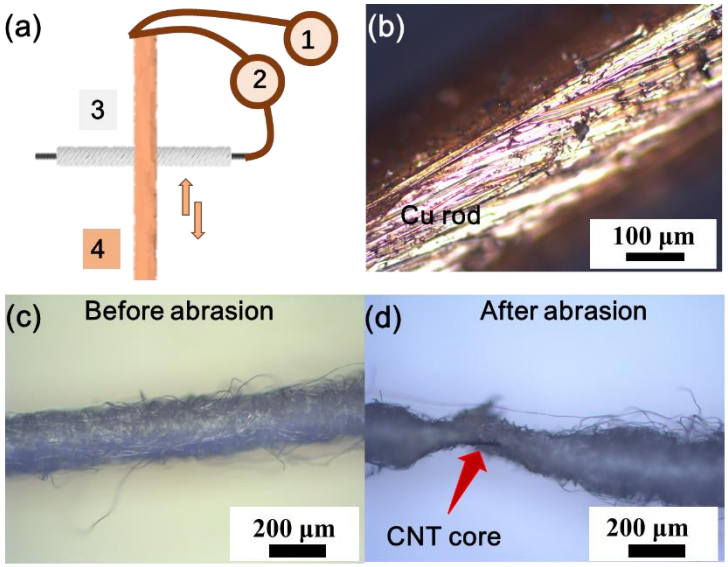

Figure S6. Wear resistance test. (a) Schematic illustration of the experimental setup. 1: Connected to a universal testing machine for monitoring friction. 2: A digital source-meter for monitoring current. 3: CNT@Silk wire. 4: Cu wire. (b) The coarse surface of the Cu wire. (c,d) Optical images of the CNT@Silk wire before (c) and after (d) abrasion.

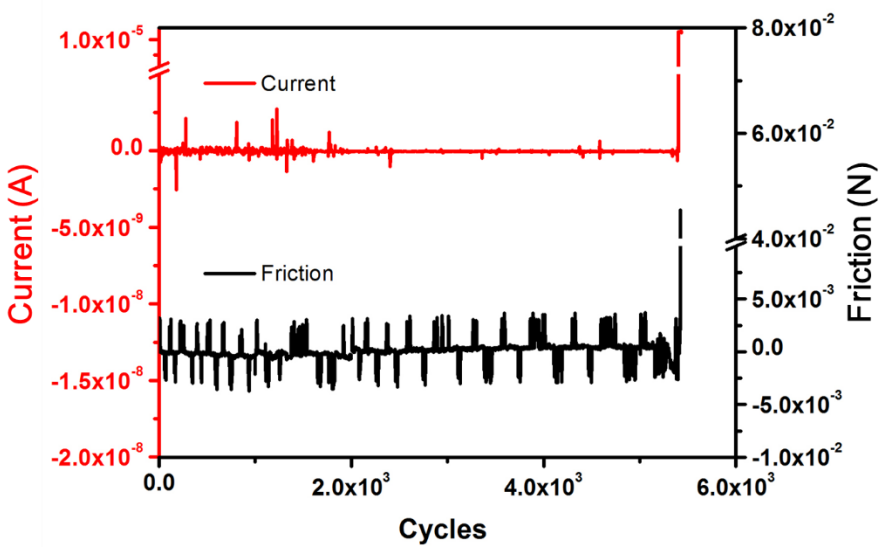

Figure S7. The current and the friction force monitored during the wear resistance test. The conductivity (red line) and the friction force (black line) between Cu rod and CNT@Silk wire. The sheath wears out at about the 5400th cycle.

Note S3. Stretchable wires

Similar to traditional fibers for fabrics, the CNT@Silk wires can be winded on elastic fibers to achieve high stretchability. Figure S8 illustrates the process to fabricate a stretchable wire based on a CNT@Silk wire and an elastic fiber. Because of the excellent flexibility of the CNT@Silk wire, it can be easily winded on other materials. In this study, we used a pre-strained Ecoflex fiber, which is a kind of skin safe elastic silicone material, as the elastic core fiber. The core fiber was pre-strained by 100% in this work. As seen in Figure S8b, with the loading of a tensile strain on the elastic wire, the distance of the neighbored coils will be enlarged and thus the integrity of the CNT@Silk wire will not be destroyed, leading to stable conductivity under high tensile strain. FIgure S8c shows the relative change of resistance of a stretchable wire under different strain, which is only of 0%, 0%, 0.03%, and 0.45% corresponding to strain of -50%, 0%, 50%, and 100%, respectively, indicating the almost stable resistance under large compression and tensile strain. Besides, the durability of the stretchable wire was tested by applying 5,000 stretching/releasing cycles of 50% strain

(Figure S8d). Due to the slight temperature increase of the wire during the long-term cycling test, the resistance of the wire showed a slight decrease. Although there is an influence of temperature, the variation of the resistance during 5,000 stretching/releasing cycles is still under 1%, showing the superior durability of the stretchable wire. The inset in Figure S8d is a magnified curve of 11 cycles (40 s), showing a very small relative change in resistance within 0.04%. The excellent mechanical stability of the conducting and stretchable wire enables its applications in highly elastic wearable electronic textiles.

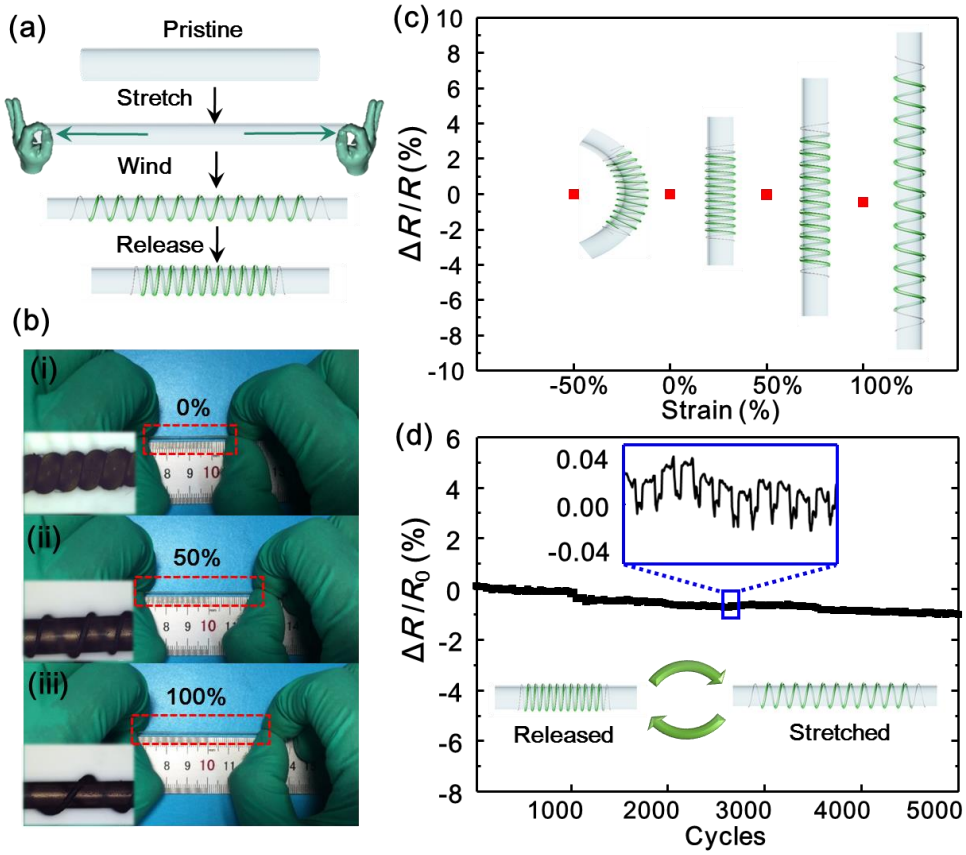

Figure S8. Fabrication and properties of a stretchable wire composed of CNT@Silk wire winding on an elastic fiber. (a) Illustration showing the fabrication of a stretchable wire. (b) Optical images of the stretchable wire under strain of (i) 0%, (ii) 50%, and (iii) 100%. The insets are magnified images. The core fiber is pre-strained by 100%. (c) Relative change in resistance of the stretchable wire under compression and tension. (d) Relative change in

resistance of the stretchable wire during 5,000 stretching/releasing cycles, showing its high electromechanical stability. The inset shows a magnified curve showing 11 cycles within 40s.

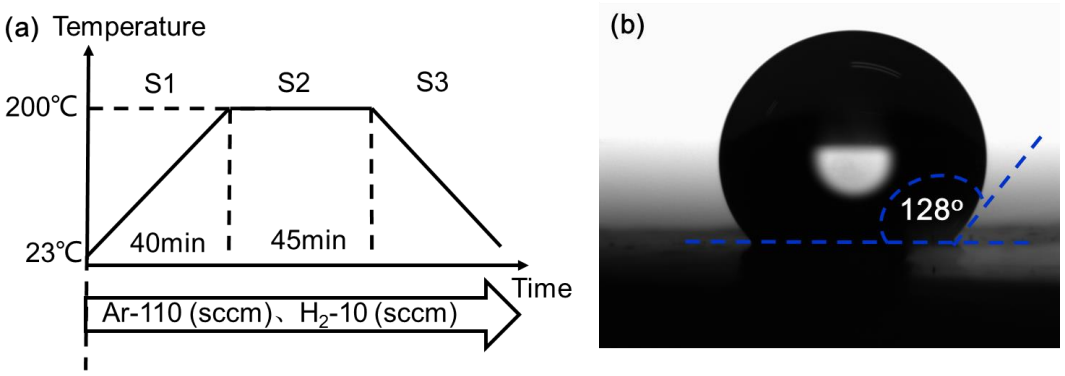

Figure S9. Heat treatment of a CNT@Silk wire and the water contact angle of a silk nanofiber film after heat treatment. (a) Annealing process including three stages: S1, ramping up the temperature, S2, annealing, S3, cooling down. (b) Water contact angle of annealed electrospun silk nanofiber membrane.

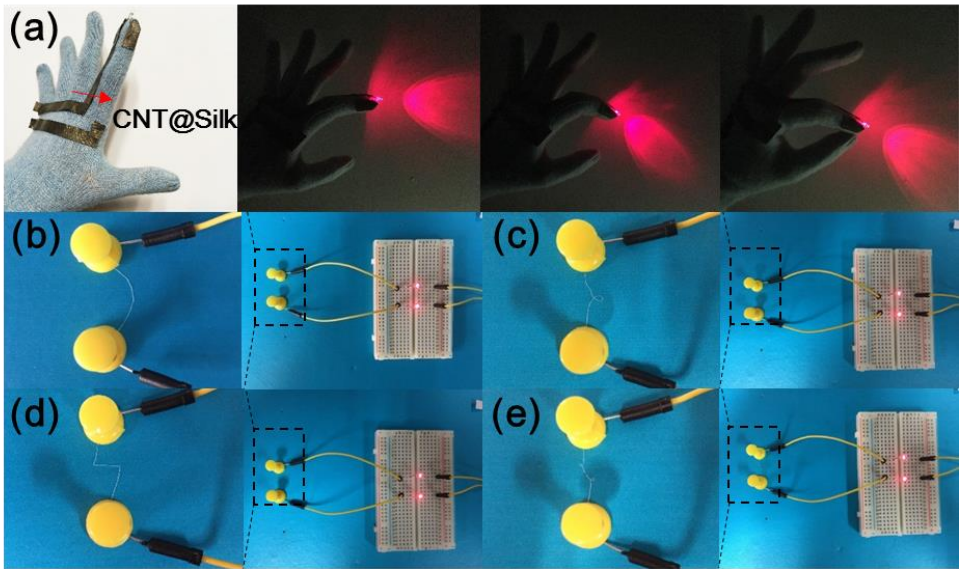

Figure S10. Optical images of red LEDs connected to a CNT@Silk wire, showing the stable conductivity of the wire under deformation. (a) Optical images showing the lit LED with the finger bending at different positions. (b-e) Optical images showing the lit LED with

different deformation of a CNT@Silk wire. (b) Arc-shaped. (c) Spiral-shaped. (d) Lighting-shape. (e) Twisted.

Note S4. Circuit Components

The LC circuit is based on the principle of electromagnetic induction. The CNT@SF coil pattern is sewed on the yoga clothes with two ends connected to a LED. The components are 1. Direct-current power source (8-12 V), 2. Wires, 3. A breadboard, 4. A CNT@SF coil (d=4 cm) with several turns, 5. A LED (red), 6. A 100 μH inductor, 7. A BD139 transistor (or equivalent), 8. A 33k resistor, 9. A 100 nF capacitor (code : 104),10. Copper coil (d=6 cm) with 2 turns. More basic information of fabricating wireless charging circuit can be refer to on the website: http://www.instructables.com/id/Easy-Wireless-LEDs/.

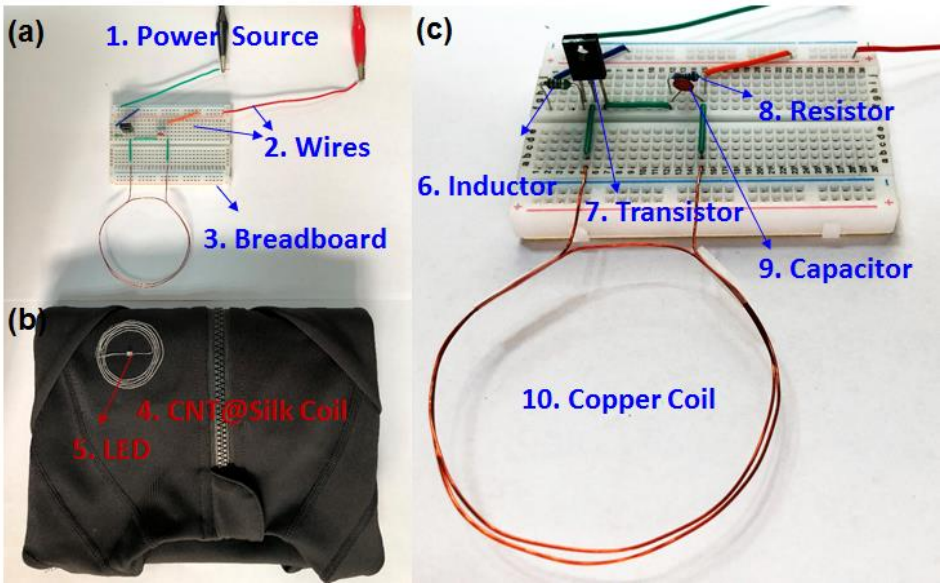

Figure S11. Optical images of the wireless charging circuit. The radio frequency emitter (a) is connected to a power source. The wireless charging receiver (b) is sewed on the yoga clothes. (c) The magnified picture of the emitter circuit.

REFERENCES

(1) Miao, M. *Particuology* **2013**, *11*, 378-393.

(2) Zhang, X.; Li, Q.; Tu, Y.; Li, Y.; Coulter, J. Y.; Zheng, L.; Zhao, Y.; Jia, Q.; Peterson, D. E.; Zhu, Y. *Small* **2007**, *3*, 244-248.

(3) Zhang, M.; Atkinson, K. R.; Baughman, R. H. *Science* **2004**, *306*, 1358-1361.

(4) Zhang, X.; Li, Q.; Holesinger, T. G.; Arendt, P. N.; Huang, J.; Kirven, P. D.; Clapp, T. G.; DePaula, R. F.; Liao, X.; Zhao, Y.; Zheng, L.; Peterson, D. E.; Zhu, Y. *Adv. Mater.* **2007**, *1*, 4198-4201.

(5) Behabtu, N.; Young, C. C.; Tsentalovich, D. E.; Kleinerman, O.; Wang, X.; Ma, A. W. K.; Bengio, E. A.; ter Waarbeek, R. F.; de Jong, J. J.; Hoogerwerf, R. E.; Fairchild, S. B.; Ferguson, J. B.; Maruyama, B.; Kono, J.; Talmon, Y.; Cohen, Y.; Otto, M. J.; Pasquali, M. *Science* **2013**, *339*, 182-186.

(6) Vigolo, B.; Penicaud, A.; Coulon, C.; Sauder, C.; Pailler, R.; Journet, C.; Bernier, P.; Poulin, P. *Science* **2000**, *290*, 1331-1334.

(7) Zhu, H. W.; Xu, C. L.; Wu, D. H.; Wei, B. Q.; Vajtai, R.; Ajayan, P. M. *Science* **2002**, *29*, 884-886.

(8) Giordano, M. A.; Schmid, S. R. *Tribol. T.* **2012**, *55*, 140-148.